

Application of Health Management and Diagnostics for Synthetic Aperture Radar (SAR) Payloads

Gregory Bower¹, Curtis Wrable¹, Ross Bird¹ and Paul Woodford²

¹*QorTek Inc., Williamsport, PA, 17701*

*gbower@qortek.com
cwrable@qortek.com
rbird@qortek.com*

²*KEYW Corporation, 7763 Old Telegraph Road, Severn, MD 21144*

pwoodford@keywcorp.com

ABSTRACT

Synthetic aperture radars are radar platforms that generate detailed images through radio frequency transmission and receiving. These systems can be high peak power, complex systems that can suffer from internal component or subsystem degradation. In addition, the operational environment can also affect the final image of the radar due to scene-based radio frequency interference (RFI). Because of these effects, it is ideal to be able to identify, classify, and quantify the degradation of these systems in order to optimize their performance and life. The work presented in this paper is an extension of QorTek's previous work using Symbolic Analysis to detect degradation using the radar's phase history data. In conjunction with the KEYW, Corp., QorTek has acquired field data to train and test its algorithm. To test the trained algorithm, a prototype hardware/software system integrating the SA approach was designed, built and flown on a test flight piggybacking on a radar system provided by KEYW. The initial results were very positive and also identified areas of improvement. The training and test results as well as the flight-test plan and results are presented in this paper. The paper concludes with specific improvements to be made to the algorithm for the next round of radar integration and flight-testing.

1. INTRODUCTION

Synthetic aperture radars are complex data-generating systems that can form intrinsically detailed images of the current environment in which the radar system operates. The deployment and testing of these systems, specifically on an

unmanned platform, can be costly and therefore it is imperative to determine if the system is operating as anticipated. It would be a significant waste of resources if the radar system was found to be not operating as intended after the mission was complete, by inspecting the data downloaded and finding it to be flawed or completely missing.

Based on this scenario, the Air Force was interested in developing approaches that could be used on Intelligence, Surveillance, and Reconnaissance systems providing operating conditions including the operating environment. QorTek has been involved in developing a data-driven approach that can detect the operating characteristics of the radar and to notify any potential issues to radar operators (Bower, 2014). These conditions include those internal to the radar system, such as component failures and external, such as RFI. The objective of the project is to detect and classify these types of degradation mechanisms and act as a means to notify personnel if issues are detected. In particular, QorTek developed the algorithm around known hardware faults in a SAR payload and with external RFI effects.

Data driven approaches are becoming more mainstream after a period of reduced research and application with numerous approaches that can be utilized (Kwok, 2014)(Schwabacher, 2005). Having access to large amounts of data and combining it with the capability to process these significant quantities of data has allowed for further interest in data-driven approaches. In essence, a data-driven approach attempts to model underlying system behaviors by utilizing data captures from the system of interest such as the application of statistics for dc-dc converter monitoring (Bower, 2011) and aircraft engines (Sarkar, 2011). The resultant system model could be statistical in nature or some other model relevant for use. The data-driven methodology

Gregory Bower, et al. This is an open-access article distributed under the terms of the Creative Commons Attribution 3.0 United States License, which permits unrestricted use, distribution, and reproduction in any medium, provided the original author and source are credited. Approved for public release: 88ABW-2015-2445

is to define the model such that the model reflects changes occurring in the system itself due to degradation and usage.

In regards to the current application, the availability of vast amounts of radar phase history data is ideal training data for a data-driven approach. This paper focuses on the further development and deployment of the algorithm and contains results from flight-testing the system in real-time with the radar in operation. The objective was to demonstrate the system operating with the radar, obtaining measures of the quality of the radar data in near real time, and to not interfere with the radar's primary function.

The paper begins with an introduction into Symbolic Analysis. This brief review can be augmented with our previous paper [Bower, 2014]. Section III describes how the SAR data is utilized in the algorithm described in Section II. Examples of training and test data are shown. Section IV investigates the training and testing of the algorithm on the RFI datasets provided to QorTek. Section V details the flight-testing including the hardware design and results obtained. The paper is concluded with Section 5 discussing the results and future work to be accomplished.

2. PROBLEM BACKGROUND

Expanding upon the work presented in [Bower, 2014], the objective was to design a system that was capable of integrating the developed software into the radar system. The software, Symbolic Analysis (SA), is briefly reviewed here.

2.1. Symbolic Analysis

Symbolic Analysis is a statistical pattern recognition tool based upon symbolic theory. Most work in the symbolic realm deals with the development of optimal models to determine the trajectory of modeled system states (Daw, Finney & Tracy, 2003). These methods are used to model complex and chaotic systems. The resultant optimal model, known as the ϵ machine, has a variable dimensional structure whose dimensions were constantly adjusted depending on the data collected over time. This variation in dimensionality made it difficult to determine deviations between models developed through system usage. In order to make meaningful comparisons between models, a machine was developed with a-priori fixed dimensional structure (Ray, 2004). This fixed dimensional machine allows for meaningful comparisons between statistical models defined at different temporal points in the system's life at the cost of optimality. The process of SA is shown in the block diagram of Figure 1. Each process will be briefly described.

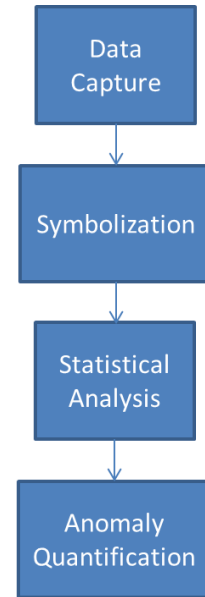


Figure 1. Symbolic analysis of time series data block diagram.

2.2. Data Capture

The data capture is an important step as it identifies data sources that are related to underlying degradation signatures. In addition to identifying relevant observables, the SA approach requires two assumptions: 1) the system does not undergo 'self-healing', and 2) that the underlying degradation dynamics can be separated from the system dynamics.

Assumption 1 forces the system to undergo a monotonically increasing degradation state, which assists in predicting future failure. Assumption 2 is far more stringent in that the data captures must be sufficiently long enough to develop statistics but also not capture changes in the underlying dynamics of the system. In other words, it is assumed that the degradation dynamics evolve at different rates than the system operates. This simplifies into a separation of scales assumption of which the SAR indeed fulfills as data rates are significantly higher than degradation signatures.

2.3. Symbolization

The next step involves transforming the time series data into the symbolic domain. This step can be thought of as a general re-quantization of the original data resulting in a coarser distribution. Symbolization requires the determination of the number of partitions to be used as well as the type of partitioning. The two most common types of partitioning include uniform partitioning (UP) and maximum entropy (ME) partitioning. QorTek has devised a new partitioning approach which combines the advantages of both UP and ME which is called Mixed (MX) partitioning.

2.3.1. Partitioning

That partitioning scheme of the algorithm allows for the collected data to be converted into the symbolic space. As stated previously, there are three main approaches utilized for this work including UP, ME, and MX although the majority of this write-up will focus on MX partitioning.

Uniform partitioning divides the range of the time series data into equal sized regions where the total number of determined partitions are defined as the set P . Given the range of the time series data as U , the partition sizes are defined as U/P and the boundaries developed from the range U . Each partition region P_i was mutually exclusive and exhaustive over the range of the data. The probabilities of the partition occurrence in the uniform case are not necessarily equal; however, the partitioning structure was equal.

The maximum entropy (ME) partitioning scheme was defined by the principle of entropy in determining the partition structures. Recall entropy as shown in Eq. 1.

$$H(X) = - \sum_{i=1}^n p(x_i) \log_2 p(x_i) \quad (1)$$

The entropy can be maximized by setting $p(x_i) = p(x_j), \forall i, j$. The logarithm to base 2 was used so that the unit of entropy is in bits. In the time series data, accomplishing maximization of entropy in the baseline case was necessary to make sure all partitions (or symbols) have equal probability of occurrence. The partition structure resulting from ME does not necessitate equal partitions as in the uniform case but does guarantee equal prior probabilities for the partitions in the baseline case. A feature of the ME partitioning scheme is that the partitions boundaries are closer in regions of the data where there are a dense number of data points. In regions where there are fewer data points, fewer partitions are generated in these areas.

Mixed partitioning was developed at QorTek to combined the sensitivity of the ME approach with the equal area distribution of the UP approach. In the work completed, the MX approach takes the desired number of partitions and divides them equally between those to be developed through ME and those to be developed under UP. The resultant MX partitioning approach very finely models regions of dense data and uniformly divides other regions to allow for evolution of the system. This became much more important when the partitioning was converted into two-dimensions. This also enables to algorithm to model slight changes in the data-dense regions while allowing for more significant system deviations through the UP partitions.

Once the partitions are defined each partition was labeled with a symbol from the alphabet S . Given a time series X of length M , if $x_i \in P_i, 0 \leq i \leq M$, then assign $s_i \rightarrow x_i, \forall i; s_i \in S$. By implementing the partition structure and assigning a unique symbol to each time series date point, the end result

was called the symbol stream. This is the re-quantized time series data that is now transformed into the symbolic domain.

2.4. Statistical Analysis

Once the partitions have been developed and symbols assigned to each partition, the next step is to construct the statistical model based on the resultant symbol stream. This step is controlled by another parameter for the SA methodology, the depth parameter D . The depth parameter controls the definition of model states from the symbol stream. States in the model are formed from D -length subsets of symbols. Therefore, the total number of states in the algorithm given the number of partitions P and the depth D is shown in Eq. (2).

$$N_s = P^D \quad (2)$$

Equation (2) holds true independent of the partitioning scheme utilized. As an example, assume a ternary partition scheme is implemented that results in three symbols; labeling them -1, 0, and 1. The methodology's resultant statistical states depend on the number of symbols in the algorithm as well as the chosen depth. The parameter depth adjusts the memory of the resultant symbolic model, that is, the parameter controls the groupings of symbols into states. For instance, if D was unity, the resultant states are 0, 1, and -1. If D was two, the resultant states would be 00, 01, 10, 11, 0-1, (-1)0, (-1)(-1), 1(-1), and (-1)1 according to (2).

Shown in Figure 2 is an example model formation with the three partition symbolic system and with D being equal to two applied to a recorded sine wave of arbitrary amplitude. These parameter choices result in a model with three states. The example sine wave in the figure is divided into zero (0), one (1) or minus one (-1) by a set threshold (partition boundary, uniform in this example). The symbol sequence is the square wave in the figure.

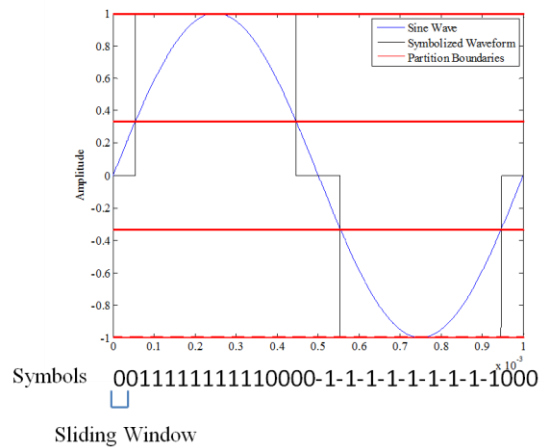


Figure 2. Example symbolization using three symbols with $d=2$ resulting in nine possible states.

With the symbol sequence s_i completed, the next step is to form states out of the symbols or groups of symbols. The probabilities of the state occurrences can be calculated and tracked across each data capture. Counting state occurrences can then be converted into probabilities to generate what is known as the State Probability Vector (SPV): the probabilities are arranged in a $N_s \times 1$ vector, where N_s represents the total number of states in the algorithm given by Eq. (2). In the case where depth of the algorithm is equal to unity, as it is in most cases, the total number of states is equal to the number of symbols used. Choosing D equal to unity results in the smallest possible model for a given number of symbols, thereby reducing computational complexity of the approach.

Once the probabilities or counts are known, a distance type metric can be applied to the baseline case and future cases to develop an anomaly based on the current system operation.

2.5. Anomaly Quantification

Anomalies inherent to degradation in the system can be generated from the use of the SPV between the data captures. The metric quantifies the deviation between the known baseline, commonly known as the healthy state of the system, and a future system state. A measure commonly used to quantify an anomaly between captures is based on the Euclidean distance given in Eq. (3) for pulse j .

$$A_j = \sqrt{\sum_{i=1}^{N_s} (z_{i,nominal} - z_{i,j})^2} \quad (3)$$

In Eq. (3), $z_{i,nominal}$ is the nominal (baseline) SPV state z_i and $z_{i,j}$ is the corresponding SPV state at iteration j . The Euclidean distance measure is used as it provides a straightforward means to measure the change between SPVs in an analysis. From this measure, it is possible to quantify anomalies present in the system and how they evolve over time and usage.

From this evolution of the anomaly, it is then possible to define a threshold of failure for the system. The threshold can then be implemented in a predictor to estimate remaining useful life of the system.

The anomaly can be used as a diagnostic measure to determine the amount of degradation the system has incurred over its lifetime or to be used as a prognostic measure. If training data exists for the system, the anomaly measure can then be used in a prognostic application to predict the remaining useful life of the system.

3. PHASE II FOCUS AND DEVELOPMENT

The Phase I program investigated applying the algorithm to previously recorded good SAR data and testing the response of the algorithm to artificially inducing degradation effects

such as adding in RFI. The results were promising which thus enable QorTek to further investigate the application of the algorithm.

Based on the results of the Phase I program, the Phase II objective was to further refine the approach and apply it to 'real world' radar data collections that could contain varying degrees of data degradation. In order to accomplish this task, QorTek teamed up with KEYW Corp., manufacturer and supplier of SAR radar systems for imaging applications. Utilizing this data, the algorithm was then tested with typical situations that a SAR radar would be involved with, namely RFI, scene variations, and hardware faults. These situations were used to train the algorithm and develop the necessary parameters that will be hardcoded into the algorithm for system implementation and operation.

An interesting aspect of radar data is that it can be contained within the frequency domain thereby providing both frequency and phase information. The original work solely focused on the frequency amplitude information ignoring the phase information. For this work, the phase information was also utilized and integrated into a two-dimensional implementation of SA where the space the algorithm operated on was now frequency magnitude and phase. This resulted in two-dimensional partitioning scheme as illustrated in Figure 3. The figure shows an example data distribution with the MX partitioning employed. Notice that there are ME partitions in the data dense regions of data with uniform partitions extending out from these ME partitions. There are an equal number of ME and UP partitions. The magnitude range of the ME partitions covers a single standard deviation of the phase history data. The remaining range was divided with UP. Note that the figure shows the I/Q representation of that data, that is:

$$d_i = a + jb \quad (4)$$

In (4), d_i is the data point defined by the complex number formed from a and b . Therefore, recall that the magnitude and phase of the data is given as:

$$|d_i| = \sqrt{a^2 + b^2} \quad (5)$$

$$\Phi_{d_i} = \tan^{-1}\left(\frac{b}{a}\right) \quad (5)$$

To obtain phase information, the regions were further divided either into two or four regions. The approach was limited to four regions in order to minimize the complexity of the model and to implement it efficiently into a GPU device.

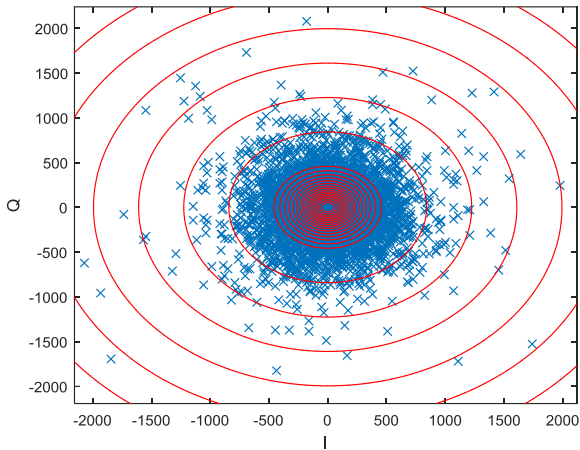


Figure 3. Two dimensional partitioning example employing the Mixed (MX) partitioning approach.

This two-dimensional approach to partitioning was also implemented completely with ME and UP approaches as well. The UP case presents a unique situation. The definition of ‘uniform’ in this case can be ambiguous. For the present case, two approaches were developed. These cases consisted of the uniform partitions being created either through uniform radius or by uniform area in which each partition has equal area. Examples for the two types of UP are shown below. The first figure, Figure 4 shown below, demonstrates the UP approach involving uniform radius circles. As can be observed, each concentric ring is equidistant from each other.

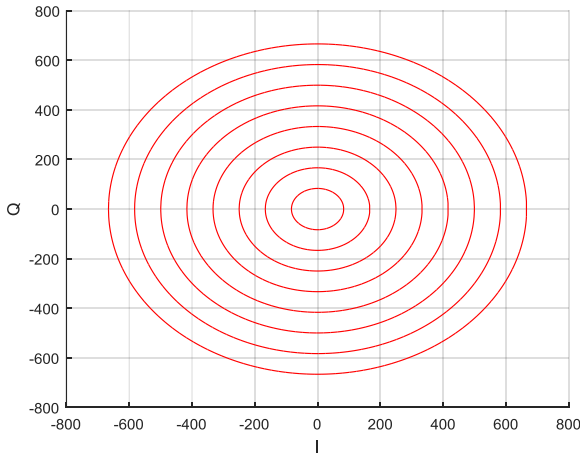


Figure 4. UP with equal radii partitions.

The following figure, Figure 5, shows the results of UP when employing equal area circles. This results in a markedly different partitioning structure. This type of UP would group the majority of data within the first or second partition region. The remaining regions would be used to identify outlier data of which RFI is typically manifested.

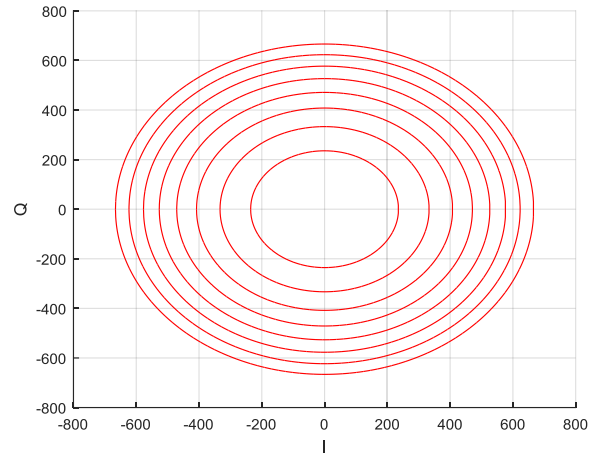


Figure 5. UP with equal area partitions.

3.1. Application to Radar

The choice of underlying partitioning depends, in part, on the degradation signatures involved in the process. In this work, the data processed by the algorithm is the phase history data of the radar. The phase history data is the frequency transformed time series sampled data of the radar returns. The resultant phase history data is truncated in the frequency domain to contain data within the bandwidth of interest.

Each pulse sent out by the radar results in a data stream related to the previously transmitted pulse. This results in a single pass containing many thousands of pulses containing significant amounts of data which can be utilized by the SA algorithm. An example distribution of the phase history data can be seen in Figure 3. An example of the collected magnitude of data is shown in Figure 6. The plot shows the magnitude of the received frequencies against each individual pulses. There is interesting RFI that can be observed in the plot.

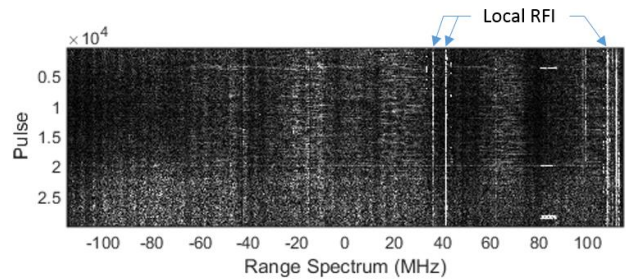


Figure 6. Example radar pass spectrum.

The SA algorithm is implemented on a pulse-by-pulse basis with the first pulse acting as the baseline for the entire pass. Each processed pulse would result in an output from the SA algorithm producing a plot for the entire pass. The output can then be used to diagnose the pass to determine if the system was operating as expected.

For diagnosis of the radar, two areas were of importance. First, the algorithm was to detect if any hardware faults had occurred within the radar and secondly, to detect pulses or passes that were significantly degraded by radio frequency interference (RFI). RFI detection will be the focus of this paper as it was the most common issue involving the radar system.

4. RADIO FREQUENCY INTERFERENCE DETECTION

RFI is a problem with SAR systems in that the final images can be corrupted due to this additional energy in certain frequency bands (Meyer, 2013)(Lord, 2005). Cell communications, TV broadcasts, and satellite transmission can all degrade the operation and final results of a SAR pass. The environment RFI can easily overwhelm the weaker SAR reflected signals. Our goal is to detect RFI issues that are contained within the phase history data without the need for image generation which can be computationally intensive. The algorithm also must not affect the operation of the radar and must minimize false positives in its output.

Detection of RFI is a challenge for numerous reasons. A straightforward example would be attempting to detect RFI by return magnitude while attempting to reject scene reflectivity changes. Datasets were given to QorTek by KEYW to explore and develop/train the algorithm on typical examples of RFI and scene reflectivity changes. A pass was completed in which the radar was pointed away from sources of RFI and then pointed towards the sources. This additional energy cause a degraded final processed image. Note that the cleaner pass still contains traces of some amount of RFI. This data was then utilized in the training of the algorithm with the results contained in the next section.

4.1. Algorithm Application to RFI

In the development of the algorithm, the data described previously was used to train the algorithm and determine the parameters (partitioning and depth) that would most efficiently be used to detect RFI. This data allowed us to further develop the two-dimensional partitioning and evaluate its capabilities beyond magnitude partitioning alone which was accomplished in [Bower 2014]. In this paper, the following results are generated utilizing the SPV and two-dimensional model formation.

The set of results utilizing the RFI corrupted data is given in Figure 7. The parameters used in the generation of the results utilized 32 magnitude partitions and four quadrant partitions. Implementing a depth of unity to minimize model complexity yields 128 model states. The baseline was chosen in the upper plot of Figure 7 used the second pulse. The partitioning approach taken was derived from the MX (Figure 3) partitioning approach. The top figure (a) relates to the pass with minimal RFI and the lower figure (b) is the pass with substantially more RFI.

Not the change in magnitude between the upper plot and the lower plot. The upper plot shows an average value around 0.04 whereas the lower plots average value is nearer to 0.01. There are some variations from pulse to pulse as would be expected and some variation from scene reflectivity although this is minimal. The larger variations observed in the lower figure are most likely due to changes in received RFI power.

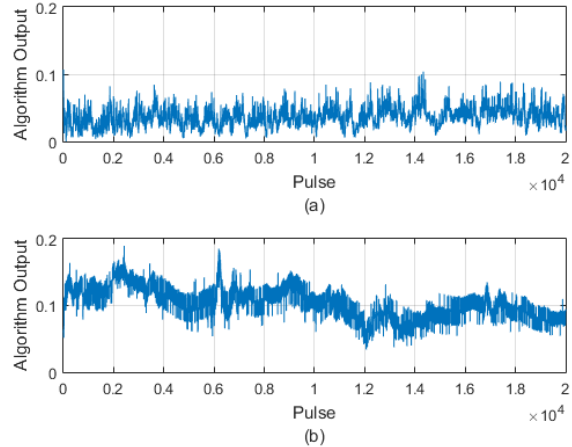


Figure 7. Algorithm output response using the MX partitioning methodology.

Utilizing the exact same data, the results for UP and ME are shown in the following two figures. The partitioning parameters were also kept constant for the UP and ME results. Both instances utilized 32 partitions. The UP was implemented with equal area regions. Four quadrant partitioning was used and the depth parameter of the SA algorithm was set to unity.

Figure 8 demonstrates the results when equal area UP was implemented. Since UP results in a system that is not as sensitive to noise in the system, the output of the algorithm contains less variation than the output with MX partitioning. The lower figure's trending also follows that obtained with MX partitioning although the spike around pulse 6,000 is absent. This is due to the sensitivity of the MX partitioning as compared to UP. The underlying trend though similar to that obtained with MX partitioning as well.

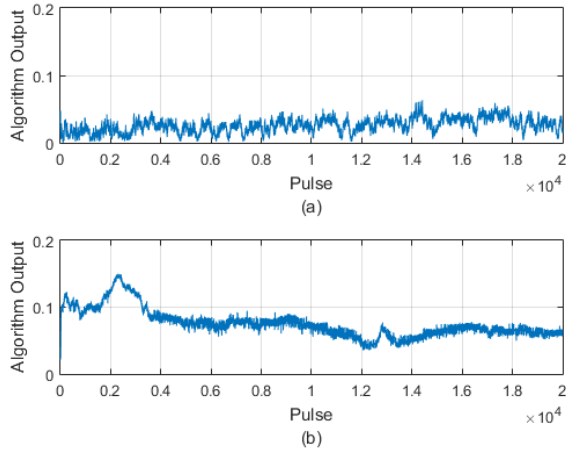


Figure 8. Algorithm output response using UP with equal area partitions.

The results in Figure 9 were generated from ME partitioning again using the same parameters for comparisons between the other two partitioning methodologies with the same radar field data. As was stated in the SA background, ME results in the most data sensitive partitioning approach and this can be observed in the results. Note the significant increase in pulse-to-pulse variation as compared to UP and MX. We originally believed this increase in sensitivity would assist in detecting degradation early, but the sensitivity to noise and data variations make it a challenge to use in typical situations. This is the primary reason for the development of the MX partitioning strategy. Again, the spike observed in the lower figure around pulse 6,000 is visible as with the case of MX partitioning.

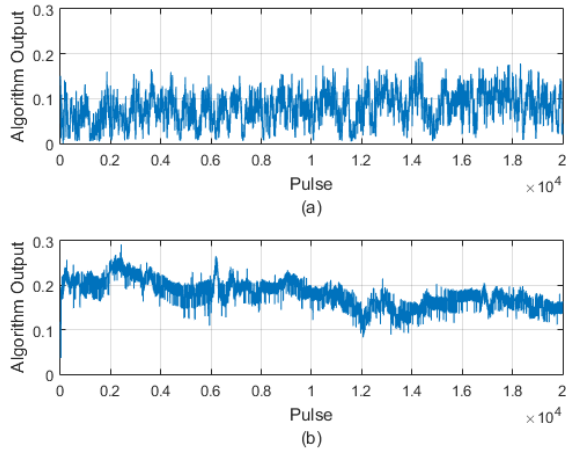


Figure 9. Algorithm output response using ME partitioning.

The above results are examples of RFI and the effect on the phase history data and on the algorithm output. Since the SA algorithm operates on the phase history data, the possibility of it being confused by normal operations can also occur.

For example, changes in the scenery reflectivity can act as a false alarm of RFI as the algorithm begins to notice the change in input data. KEYW was gracious enough to supply QorTek with an example of this event. The dataset was obtained from a collected pass that transitioned into land. An example of this is the Webster Field pass of which the developed SAR image is shown in Figure 10.

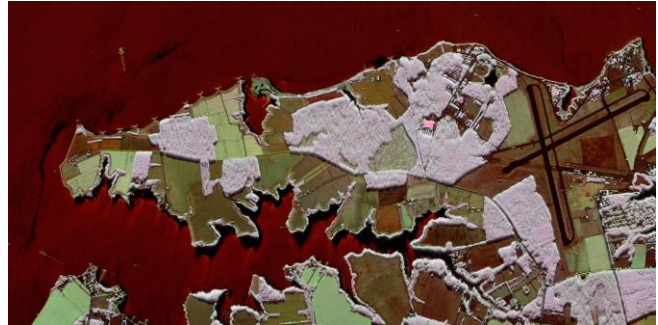


Figure 10. Webster Field SAR image. Courtesy of The KEYW, Corp.

The interesting scenery features that can cause the issue is with the radar transitioning from the bay/water onto land. Water and land have very different radar reflectivity, so the statistics of the collected radar data change significantly when the illuminated scene changes from mostly water to mostly land. Changes in land use, for example from rural to urban, can also generate false alarms. Figure 11 shows the results using the CBBT data and the ME partitioning approach. The figure shows some variation in the algorithm output with the occasional pulse outlier. An interesting strong signal is detected just before pulse 200,000. This is due to a strong reflector in the scene which was identified as a ship.

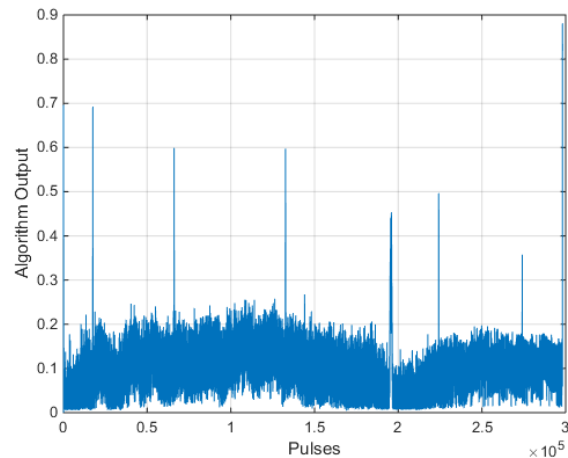


Figure 11. Algorithm output using 32 ME regions with four quadrants on CBBT dataset.

Figure 12 follows the ME results with the MX partitioning methodology. The results, as expected, are very similar to the ME results due to sensitivity of both approaches. This indicates that the data is mostly focused within the ME partitions within the MX partitioning. Again, the same strong reflector is observed in this figure as was observed in the previous figure. The output magnitude is also different due to the change in generated statistics between ME and MX partitioning. The final figure, Figure 13, shows the results utilizing the uniform partitioning approach with equal area regions.

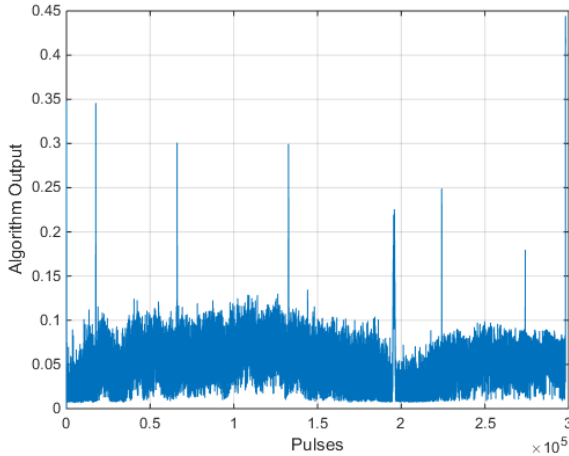


Figure 12. Algorithm output using 32 MX regions with four quadrants on CBBT dataset.

The results in the figure show some interesting features. First, the strong reflection received in the pulses before pulse 200,000 is clearly visible within the figure. In addition, the output increases towards the end of the pass. This increase is due to the radar platform moving from sea to land with a general change in scenery reflectivity. This is an interesting result as the two previous approaches did not clearly show the change in reflectivity. The reduced sensitivity of the UP approach allows this detail to be more pronounced than in both the MX and ME partition implementations.

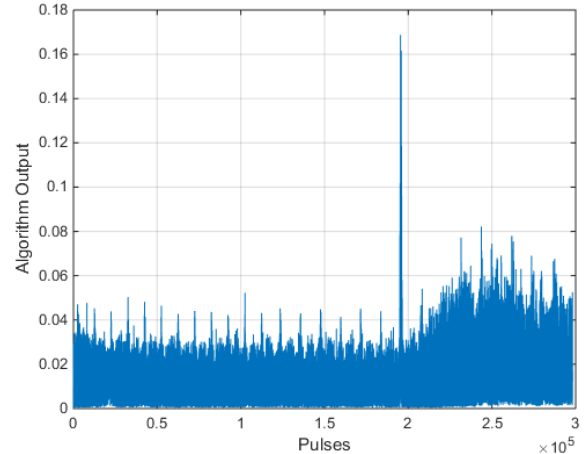


Figure 13. Algorithm output using 32 UP equal area regions with four quadrants on CBBT dataset.

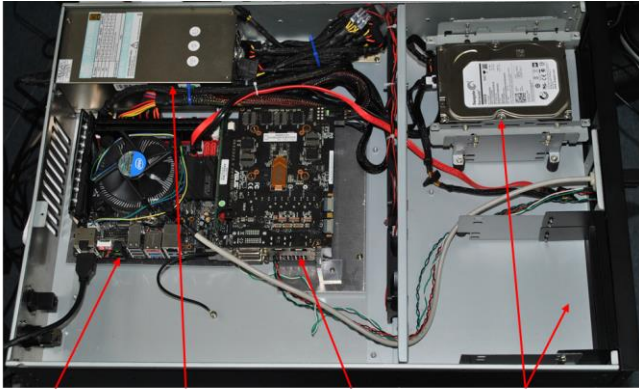
Observing the above three different results for each type of partitioning is the reason why the algorithm approach for the radar integration will utilize all three partitioning strategies. Each approach has its benefits and can detect different features as detected from the scene. This information can then be used to further diagnose issues with the data and/or radar payload. The question of whether it was scenery change or RFI can be determined by utilizing all three approaches whereas scenery changes are more clearly indicated by UP. To determine the difference between a strong reflector or RFI, the approach requires the use of the state transition matrix (Bower 2014) and frequency information (band) to determine if it is RFI or a strong reflector. Indeed, a scenery change is very gradual as compared to a strong reflector/RFI.

The above practical examples allowed us to refine the algorithm and prepare it for initial prototype testing on the radar system.

5. PROTOTYPE FLIGHT TESTING

A primary goal of the Phase II program was to develop the hardware and software systems needed to integrate the system onto a SAR platform. Given that the system would be involved in significant data processing, the hardware platform chosen for the process was GPU based to allow for a highly-threaded implementation of the algorithm.

A high-end gamer PC system was utilized for the work to achieve the necessary throughput needed to keep up the radar. The system consisted of a Core i7-4770k with 16GB system RAM and an NVidia GTX670 with 2GB of onboard GRAM. The entire system was inserted into a 2U-compatible 19" rackmount system (Figure 14). The SA algorithm was written in CUDA/C and the support routines written in C#.



Mini-ITX Power Supply GeForce GTX670 Hard Drive Bays

Figure 14. Rack mount computer prototype to integrate with radar system for testing.

The system was designed to allow for expansion specifically in the area of storage in case it was needed. The power required was also carefully designed to be within specification of the available power onboard the aircraft. The most significant power draw was the GTX670 which at full power can consume 170W. The CPU load was minimized in order to reduce the total power required by the added hardware. To further reduce power and the chance of problems, a 256GB solid state drive was utilized as the main hard drive for the test setup.

The hardware was then installed into the radar rack system (Figure 15) and connected into the system via 1000BASE-T network. The gigabit connection was necessary in order to download and process the radar data as it was being recorded and to enable the system to keep up with the radar.

The goal of this flight test was to demonstrate that the system can be integrated into the radar payload without affecting its operation or causing any other atypical operation, and to also demonstrate the capabilities of the SA algorithm in real time. It was discovered that the instantaneous output of the SA could be used for RFI detection during flight.



Figure 15. QorTek hardware payload installed in radar rack for flight testing.

The flight path was through the Naval Air Station Patuxent River area. The flight tests took place on July 1st – 2nd, 2014 and consisted of a couple of passes. The testing was carried out for a pre-mission systems check and verification by KEYW. QorTek joined the KEYW team to test out the diagnostic hardware and software.

The first day of flights went as expected with the diagnostic hardware without any major issues. The results shown below implement 32 UP regions utilizing equal area. This partition structure was chosen to be implemented in the first test run as it performed equally well in all situations during algorithm development. The next revision of the SA algorithm code will include the other partition types.

The first example of results is shown in Figure 16. This data was taken from pass 212616 from the L-band with VH polarization. The data connection that QorTek had access to was the horizontally-polarized receive portion of the data. All of the following results were thus taken from the *H available polarization channels.

The results show minimal issues in the data with the exception of a single pass outlier around pulse number 6,000. A more interesting example is shown in Figure 17 and Figure 18 taken from the second day of testing.

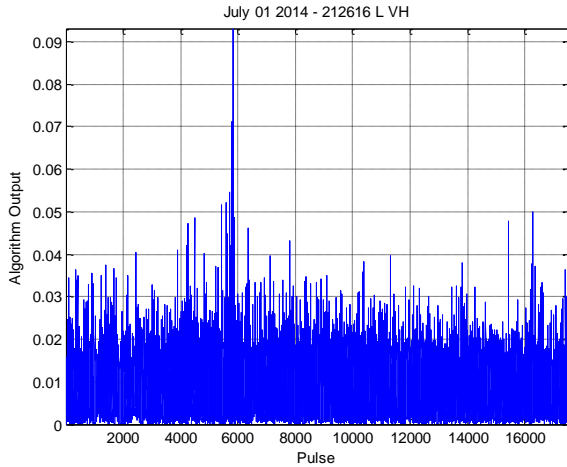


Figure 16. Example result from the first flight test using pass 212616 and the L-band VH channel.

The results shown in Figure 17 were taken from the second day of testing and from the PHH channel of data. The majority of data is indicated as normal until around pulses 7,500 – 8,500. The algorithm output begins to increase and decrease back down to the expected value. This is indicative of RFI or some other corrupting signal present in the data. To determine if this RFI was limited to the P-band, the next figure contains the results for the L-band channel.

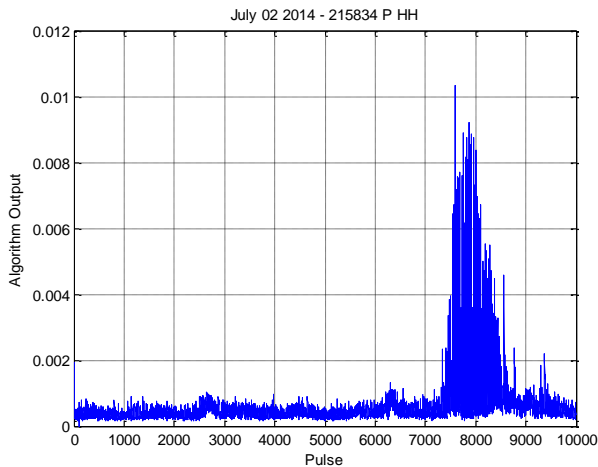


Figure 17. Example result from the first flight test using pass 215834 and the P-band HH channel.

Figure 18's results do not show the same behavior during those periods indicating a P-channel related RFI event that has occurred during the data collection during the pass. In this case, the event was isolated mostly to the P-band radar. The source of the RFI was unknown in this case but occurred at a frequency of 425MHz and was periodic. It was also confirmed to be absent from the L-band data.

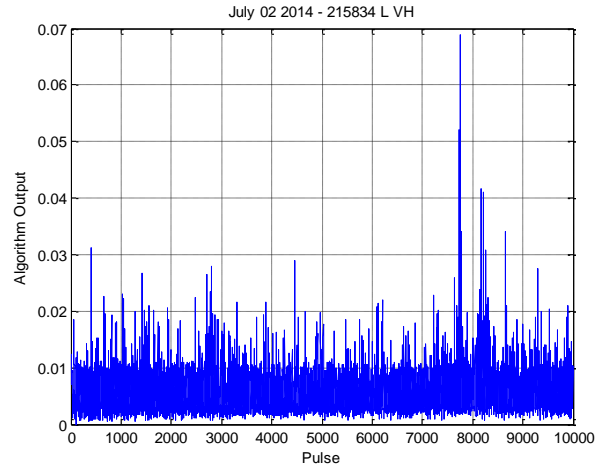


Figure 18. Example result from the first flight test using pass 215834 and the L-band VH channel.

The above two figures are an excellent example of RFI. Note that *nearly all* passes are going to contain some amount of RFI which is what introduces some of the pulse-to-pulse variability in the output.

The detection of RFI in one band and not in the other was an excellent indicator of algorithm performance for QorTek. Some issues that occurred during testing included long processing times needed to pull data from the data arrays on the radar. This problem is being addressed for the next flight test.

6. CONCLUSION

The SA algorithm has been shown to indicate possible issues with the operation of a Synthetic Aperture Radar (SAR) payload through statistical observation of the phase history data. Of importance to the program was to identify the type of degradation, whether it is internally based due to hardware degradation or externally, environmentally sourced. The data shown contained RFI issues, the most common problem with these systems. The algorithm was trained and tested on these example data sets as provided by KEYW and then implemented into a flight test.

The flight testing of the prototype was a success in that it was able to obtain and process the radar phase history data from the radar while it was in operation. The algorithm itself did not negatively impact the operation of the radar and the results produced interesting features.

The next goal of the program is to identify the RFI to assist in radar operation. In addition, the algorithm will continue to be used to also detect the possibility of hardware problems. KEYW has provided example data sets that contain hardware problems that were also trained and tested in the algorithm. Although much more uncommon, these degradation features will also be programmed into the final algorithm

implementation. The final objective of the program is to complete a second flight test of the improved algorithm that decreases its execution time and reduces the size, weight, and power impact to the host payload.

ACKNOWLEDGEMENT

This work was supported by an AFRL contract FA8650-13-C-2318. QorTek would also like to thank Thierry Pamphile AFRL Wright-Patterson for his support and guidance during this work. QorTek would like to acknowledge the support from NAVAIR for the permission to test the prototype on a flight and for the data presented in this work.

NOMENCLATURE

A	=	anomaly
D	=	symbolic depth
d_i	=	complex data point
$H(\cdot)$	=	entropy
MX	=	mixed partitioning
ME	=	maximum entropy
N_s	=	number of states
$p(\cdot)$	=	probability
P_i	=	i^{th} partition
s_i	=	i^{th} symbol
RFI	=	radio frequency interference
U	=	time series data amplitude range
UP	=	uniform partitioning
X	=	time series data
z	=	state probability vector

REFERENCES

- Bower, G., Mayer, J., & Reichard, K. (2011). "Symbolic Dynamics and Analysis of Time Series Data for Diagnostics of a dc-dc Forward Converter," in *Annual Conference of the Prognostics and Health Management Society*, Montreal, 2011.
- Bower, G., Zook, J., Bird, R. (2014). "Health Management and Diagnostics for Synthetic Aperture Radar (SAR) Payloads" in *Annual Conference of the Prognostics and Health Management Society*, Fort Worth, 2014.
- Daw, C.S., C.E.A. Finney & E.R. Tracy (2003). "A review of symbolic analysis of experimental data." *Review of Scientific Instruments* 74.2 (2003): 915-930.
- Kwok L. Tsui, Nan Chen, Qiang Zhou, Yizhen Hai, and Wenbin Wang (2014), "Prognostics and Health Management: A Review on Data Driven Approaches," *Mathematical Problems in Engineering*, Article ID 793161, in press.
- Lord, R. T. (2005) "Radio Frequency Interference Suppression applied to Synthetic Aperture Radar Data", XXVIIIth General Assembly of International Union of Radio Science, URSI 2005, New Delhi, India.
- Meyer, F.J.; Nicoll, J.B.; Doulgeris, A.P., (2013) "Correction and Characterization of Radio Frequency Interference Signatures in L-Band Synthetic Aperture Radar Data," *IEEE Transactions on Geoscience and Remote Sensing*, vol.51, no.10, pp.4961-4972.
- Ray, Asok (2004). "Symbolic dynamic analysis of complex systems for anomaly detection." *Signal Processing* (2004): 1115-1130.
- Schwabacher, M. 2005. "A Survey of Data-Driven Prognostics." *Proceedings of the AIAA Infotech@Aerospace Conference*. Reston, VA: American Institute for Aeronautics and Astronautics, Inc.
- Sarkar S, Jin X, Ray A. (2011) "Data-Driven Fault Detection in Aircraft Engines with Noisy Sensor Measurements." *ASME. J. Eng. Gas Turbines Power*.

BIOGRAPHIES

Gregory Bower is currently the CTO of QorTek Inc. in Williamsport, PA. He received his B.S., M.S., and Ph.D. degrees in Electrical Engineering all from The Pennsylvania State University. Previously, he had worked as an assistant with the Applied Research Laboratory in State College, PA. His research interests include Prognostics and Health Management (PHM) of electronic systems, robust and optimal control theory, system identification, and power conversion.

Curtis Wrable is currently an Integrated Systems Engineer at QorTek Inc. in Williamsport, PA. He received his B.S. in Electronics Engineering from Pennsylvania College of Technology in 2009. Over the past six years, Curtis has worked on a number of different research areas over the course of his career including: analog and digital design, piezoelectrics, power electronics, and automated testing systems. His research interests include the areas of PCB layout and design, development of embedded systems, and generating software solutions to critical engineering problems.

Ross Bird is currently the President of QorTek, Inc. He received his B.S. in Electronics from Penn State in 2001, he then received his MSEE in 2003. Over the past decade Mr. Bird has worked extensively at the leading edge of power electronics design (holding several patents and additional pending in this technology); that incorporate advanced materials, design and digital control. He has extensive experience in the design and development of advanced power modules and has been lead developer of such power. His research interests include the areas of digital design and microcontrollers, digital implementation of complex numerical algorithms and mixed A/D PCB layout and design.

Paul Woodford is a Principal Research Engineer at KEYW Corporation in Severn, MD. He received the B.S. degree in electrical engineering from Bucknell University in 1989 and the M.S. and Ph.D. degrees in electrical and computer engineering from Carnegie Mellon University in 1991 and 1995, respectively. He worked at Essex Corporation from

1995 to 2007, and at Northrop Grumman Corporation from 2007 to 2011. His interests are in the areas of synthetic aperture and moving target imaging and exploitation. He holds two U.S. patents for radar signal processing.